DØ Note 6179-CONF

Search for the Standard Model Higgs boson in the $\mu + \tau_{\rm had}$ final state with 7.3 fb^{-1} of $p\overline{p}$ collisions at $\sqrt{s} = 1.96$ TeV

The DØ Collaboration
URL http://www-d0.fnal.gov
(Dated: March 11, 2011)

We present a search for the Standard Model (SM) Higgs boson (H) in events of low jet multiplicity with high p_T muons and taus events with large missing transverse energy in $p\overline{p}$ collisions at a center-of-mass energy of $\sqrt{s} = 1.96$ TeV. The data have been collected from April 2002 to July 2010 with the DØ detector and correspond to an integrated luminosity of 7.3 fb^{-1}. No excess above the expected SM background is observed and we set 95 % C.L. upper limits on $\sigma(p\overline{p} \to HX) \times \mathcal{BR}(HX \to \mu\tau)$ as ratios to the SM cross section between 6.6 to 24 for Higgs masses from 135 to 200 GeV.

Preliminary Results for Winter 2011 Conferences

I. INTRODUCTION

Electroweak symmetry breaking is one of the cornerstone of the Standard Model (SM) and the associated remnant degree of freedom, the Higgs boson, remains undiscovered so far. Electroweak precision measurements and consistency of the SM constrain the Higgs boson mass to be 89^{+35}_{-26} GeV at 68 % C.L. [1] while direct searches at LEP and Tevatron impose $m_H > 114.4$ Gev [2] and exclude a Higgs boson mass between 158 and 175 GeV [3].

If the SM Higgs boson mass is large (higher than $m_H \gtrsim 135$ GeV), we can benefit from the relatively large production cross section of the process $gg \to H \to WW$ due to the very high $H \to WW$ branching ratio. The predicted cross section is $\sigma(gg \to H \to WW) = 0.37$ pb in 1.96 TeV $p\bar{p}$ collisions for $m_H = 165$ GeV [5, 6]. In this final state, the leptonic decays of the W bosons produce a clear signature in the detector. The most sensitive channels are $e\mu, ee, \mu\mu$. Di-leptons final state involving τ leptons are more challenging due to the decay of the τ lepton inside the detector and have less sensitivity because of the large instrumental background. Events in which both τ leptons decay leptonically are analyzed in the ee, $e\mu$ and $\mu\mu$ final states

However, due to the high branching ratio of τ leptons into hadrons (65 %), final states involving hadronic τ decay ($\tau_{\rm had}$) bring a significant amount of signal events. We hereafter present a search for the Standard Model Higgs boson decaying to a muon, a hadronically decaying τ lepton and missing transverse energy. This search can benefit from other Higgs boson signal contributions such as vector boson fusion and associated production in addition to the gluon fusion production mode.

The DØ experiment has produced several searches for SM Higgs bosons in the $e\mu$, $\mu\mu$ and ee final state [7], the $\mu + \tau_{\rm had}$ channel is looked for in the data collected by the DØ detector. A previous analysis of this final state was presented in [4]. This new analysis considers a dataset corresponding to an increase of a factor 7 in the integrated luminosity and uses a multivariate technique to increase the sensitivity to a possible signal. Relative to the previous analysis [4] we obtain at least a gain of a factor 2.7 in sensitivity at $m_H = 160$ GeV.

II. DATA AND MONTE CARLO SAMPLES

The data used in this analysis were recorded between April 2002 and July 2010. After data quality requirements, the total data sample corresponds to an integrated luminosity 7.3 fb^{-1} [8]. A description of the DØ detector and its triggering system can be found in [9]. In this search, we select events based on a mixture of single and dilepton triggers and of triggers requiring both lepton and jet signatures. However, to derive the corresponding trigger efficiency, we rely on events triggered by high p_T muons. These triggers have a known efficiency (around 65 %) measured in $Z \to \mu\mu$ events. In our inclusive trigger approach, the typical trigger efficiency is of the order of $90-100\%$ and mainly depends on the reconstructed τ candidate transverse momentum.

Signal samples are generated for Higgs boson masses between 115 and 200 GeV using the event generator Pythia [10]. We consider the gluon fusion, vector boson fusion and associated production (WH, ZH) processes. The signal cross sections are calculated at NNLO for gluons fusion and associated production [5, 6, 11] and at NLO for vector boson fusion [12]. The Higgs boson decay branching ratios are computed with Hdecay [13].

The dominant sources of background are W+jets, $t\bar{t}$, dibosons, multijet (MJ) and Z+jets production. In MJ events, the muon primarily comes from semileptonic b hadron decays, while the τ is faked by a jet. Except for MJ and W+jets contributions, all backgrounds are estimated using Monte Carlo simulations: Alpgen [14] is used to estimate $t\bar{t}$ and Z+jets backgrounds while the diboson processes are generated using Pythia.

The event generators are used with the Cteq6l1 [15, 16] parton distribution functions (PDF). Alpgen samples are processed through Pythia for showering and hadronization. τ lepton decays are modelled with Tauola [17]. All samples are then passed through a Geant-based [18] simulation of the DØ detector. Data from a random beam crossing are added to Geant events to model effects of detector noise, pileup, and additional $p\bar{p}$ interactions. The combined output is processed through the same reconstruction algorithms as the data.

Corrections accounting for differences between data and the simulation are applied to the simulated events. They are derived from control data samples and correct for object identification efficiencies, trigger efficiencies, primary $p\bar{p}$ interaction position (primary vertex), object energy scale, and the transverse momentum spectrum of Z bosons. After applying all corrections, the yields for signal and backgrounds are calculated as the product of the acceptance (from the simulation) times the luminosity and theoretical cross sections.

III. EVENT RECONSTRUCTION AND SELECTIONS

This analysis involves the reconstruction of muons, hadronic decays of τ lepton ($\tau_{\rm had}$), jets and missing transverse energy ($\not\!\!E_{\rm T}$) arising from escaping neutrinos.

Muons are identified using track segments reconstructed in the muon system and are matched to a track reconstructed in the inner tracking system. Hadronic τ decays are identified [19] as energy deposits in the calorimeter, reconstructed with a jet cone algorithm $\mathcal{R} = 0.3$ [20], which have associated tracks. $\tau_{\rm had}$ candidates are then split in three different categories: one-prong τ decay with no π_0 (called $\tau_{\rm had}$ type 1), one-prong decay with π_0 ($\tau_{\rm had}$ type 2) and multiprong decay ($\tau_{\rm had}$ type 3). In addition, we use a neural network (NN$_\tau$) based τ identification to separate quark or gluon jets from genuine $\tau_{\rm had}$ [19]. NN$_\tau$ is based on shower shape variables, isolation variables and correlation variables between the tracking and the calorimeter energy measurements. The vectorial missing transverse energy is the negative of the vector sum of the transverse energy of calorimeter cells satisfying $|\eta| < 3.2$. We correct the vectorial quantity for the energy scales of reconstructed final state objects, including muons. The missing transverse energy $\not\!\!E_{\rm T}$ is defined as the norm of the vectorial missing transverse energy. Jets are reconstructed from energy deposits in calorimeter towers using the midpoint cone algorithm with a radius $\mathcal{R} = 0.5$ [20]. Jet reconstruction and energy scale determination are described in detail in Ref. [21]. All calorimeter jets are required to pass a set of quality criteria with about 98% efficiency and there must be at least two reconstructed tracks within $\Delta\mathcal{R}$(track, jet-axis) $= \sqrt{(\Delta\eta)^2 + (\Delta\varphi)^2} < 0.5$ (where η is the pseudo-rapidity and φ the azimuthal angle). Jets are also required to have at least two tracks originating from the primary vertex.

A. Preselections

In a first step we select a background-dominated sample by requiring:

- one primary vertex with at least three tracks;
- exactly one isolated muon with $p_T(\mu) > 15$ GeV and $|\eta| < 1.6$;
- exactly one $\tau_{\rm had}$ with a transverse momentum, as measured in the calorimeter, $p_T(\tau) > 12.5/12.5/15$ GeV for type type 1/2/3, and $|\eta_{\tau_{\rm had}}| < 2.0$. Additionally, the tracks attached to the $\tau_{\rm had}$ candidate must satisfy: $\sum_{trk} p_T(trk) > 7/5/10$ GeV, where $p_T(trk)$ is the track transverse momentum as measured by the tracking system, for $\tau_{\rm had}$ type 1/2/3 respectively. For type 3, the leading track must have $p_T > 7$ GeV. $\tau_{\rm had}$ candidates matching any reconstructed muon within $\Delta\mathcal{R} < 0.5$ are discarded. $\tau_{\rm had}$ type 3 candidates having $Q_{\tau_{\rm had}} = 0$ are rejected. NN$_\tau$>0.9/0.9/0.95 is required for $\tau_{\rm had}$ type 1/2/3 respectively; this tight identification criterion has an overall efficiency of ≈ 55 % in signal events for a fake rate of ≈ 2 % in multijet events;
- the electric charge of the $\tau_{\rm had}$ ($Q_{\tau_{\rm had}}$) must be opposite to the one of the muon (Q_μ), *i.e.* $Q_\tau \times Q_\mu < 0$.

To ensure a proper combination with other Higgs boson searches, we require the following additional criteria which makes this analysis orthogonal to the others:

- events with a reconstructed electron satisfying $M_T^{\rm min}(l, \not\!\!E_{\rm T}) > 20$ GeV, as defined in Eq. (1), where $l = (e, \mu)$, are removed (orthogonality with the $H \to WW \to e\mu\nu\nu$ search [7]).
- events with at least one jet with $p_T > 20$ GeV and a second jet with $p_T > 15$ GeV are rejected (orthogonality with the $H(\to \tau\tau)jj$ search [22]).

$$M_T^{\rm min}\ (l, \not\!\!E_{\rm T}) \ \equiv\ {\rm Min}[M_T(l_1, \not\!\!E_{\rm T})\,,\ M_T(l_2, \not\!\!E_{\rm T})] \tag{1}$$

$$M_T(l_i, \not\!\!E_{\rm T}) \ =\ \sqrt{2\,|p_T^{l_i}|\,|\not\!\!E_{\rm T}|\ (\ 1 - \cos\Delta\varphi(l_i, \not\!\!E_{\rm T})\ )} \tag{2}$$

The preselection sample is dominated by Z+jets, W+jets and MJ backgrounds. The MJ contribution is evaluated from data using different methods presented in the next section III B. The W+jets background is estimated from the simulation corrected using a data-driven method described in section III B. Tab. I gives the expected and observed numbers of event at the preselection level while Fig. 1 shows $p_T(\tau)$ and $M_{\rm vis}$ distributions, with:

$$M_{\rm vis} = \sqrt{(|\vec{p}_\tau| + |\vec{p}_\mu| + \not\!\!E_{\rm T})^2 - \left(\vec{p}_\tau + \vec{p}_\mu + \vec{\not\!\!E}_{\rm T}\right)^2}. \tag{3}$$

	$\tau_{\rm had}$ type 1	$\tau_{\rm had}$ type 2	$\tau_{\rm had}$ type 3	all types
$Z(\rightarrow \tau\tau)$	1233 ± 15.2	8294 ± 37.8	1902 ± 17.6	11430 ± 44.4
$Z(\rightarrow \mu\mu/ee)$	156 ± 4.5	910 ± 11.1	148 ± 3.8	1215 ± 12.6
$W(\rightarrow \mu\nu)$	368 ± 11.5	1285 ± 18.3	944 ± 13.0	2598 ± 25.2
$t\bar{t}$	6.0 ± 0.2	42.9 ± 0.5	5.8 ± 0.2	54.8 ± 0.6
diboson	38.7 ± 0.9	219 ± 2.1	35.6 ± 0.9	293 ± 2.5
QCD	396 ± 15.0	1434 ± 23.2	1067 ± 20.2	2898 ± 34.3
Exp. background	2198 ± 24.7	12188 ± 49.3	4104 ± 30.1	18491 ± 62.8
Data	2242	12534	4180	18956
Higgs 165 GeV	0.9 ± 0.0	5.0 ± 0.1	0.7 ± 0.0	6.6 ± 0.1

TABLE I: Expected and observed numbers of events at the preselection.

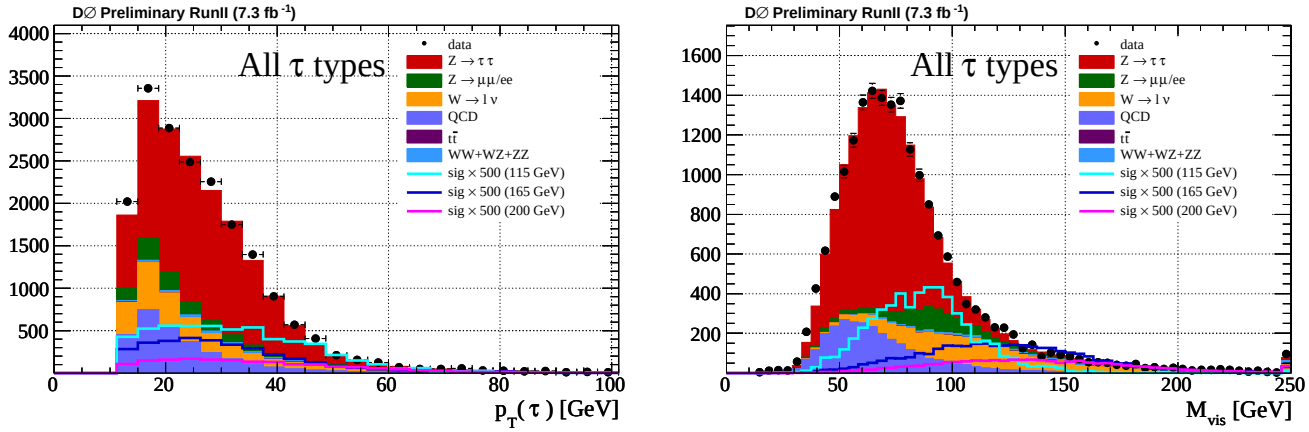

FIG. 1: Data versus MC comparison of $p_T(\tau)$ and $M_{\rm vis}$ distribution at the preselection level for all $\tau_{\rm had}$ types.

B. Multijet and W+jets background estimation

In MJ events, the muon candidate primarily comes from semileptonic decays of b hadrons while the $\tau_{\rm had}$ candidate is faked by a jet. In the W+jets background, the muon candidate is an isolated muon coming from the W decay while the $\tau_{\rm had}$ candidate is faked by the recoil jet.

We developed two different methods to estimate the MJ background from data named respectively Same-Sign Method (or $f_{OS/SS}$) and Isolation Method (or $f_{\rm Iso/NoIso}$). The former one is considered to estimate the systematic uncertainty on this prediction while the latter one is used to predict the nominal MJ distribution.

- *the Same-Sign method.* The charge correlation between the muon and the $\tau_{\rm had}$ candidates is expected to be small in the MJ background. Hence, we expect a similar amount of events with $Q_{\tau_{\rm had}} \times Q_\mu < 0$ (OS for Opposite Sign) and $Q_{\tau_{\rm had}} \times Q_\mu > 0$ (SS for Same Sign). The MJ background is determined from a data sample satisfying the preselection requirements except the charge correlation which is reversed. The other expected SM backgrounds are subtracted from this SS sample, and the number of MJ events in the OS (signal) sample is obtained by multiplying the SS sample by the factor $f_{OS/SS}$, computed in a MJ control sample selected by requiring NN$_\tau$< 0.2 and $m_T(W) < 30$ GeV. $f_{OS/SS}$ is found to be 1.10/1.08/1.08 ± 0.02/0.01/0.01 for type 1/2/3.

- *the Isolation Method method.* This method is based on a non isolated muon sample obtained by reversing the muon isolation criteria. This high statistics, very pure, MJ sample does not describe accurately some kinematic variables when compared with the MJ background in the isolated (signal) sample. To take into account those differences, we derive a scale factor $f_{\rm Iso/NoIso}$ which depends on the relevant kinematic variables. $f_{\rm Iso/NoIso}$ is measured in a control sample selected by requiring NN$_\tau$< 0.2 and $m_T(W) < 30$ GeV and the dependence with $p_T(\tau)$, $\not\!\!E_{\rm T}$ and $p_T(\mu)$ are taken into account. Eventually, the normalization is measured with the $f_{OS/SS}$ method.

The W+jets background is the dominant background in the search presented here. In this case, the reconstructed muon is coming from the $W \rightarrow \mu\nu_\mu$ decay, while a jet in the event fakes a hadronically decaying τ lepton. This $\tau_{\rm had}$ fake

rate is not well predicted by the simulation and can be measured in the SS (signal free) data. This approach assumes that the simulation provides a good modelling of the OS over SS ratio in W+jets events. While we could expect $Q_{\tau_{\rm had}}$ and Q_μ to be independent (*i.e.* OS over SS ratio of 1), the electric charge correlation between the reconstructed $\tau_{\rm had}$ and the muon from the W is an important effect in those events. First, there are Feynman diagrams implying a large charge correlation between the recoiling parton q and the W in Wq production. Then, we observe a correlation between the charge of parton q and the reconstructed $\tau_{\rm had}$ which strongly depends on NN_τ. The convolution of these two effects leads to a specific NN_τ-dependence of OS over SS ratio according to the $Q_{\rm parton} \times Q_\mu$ value, as shown in Fig. 2.

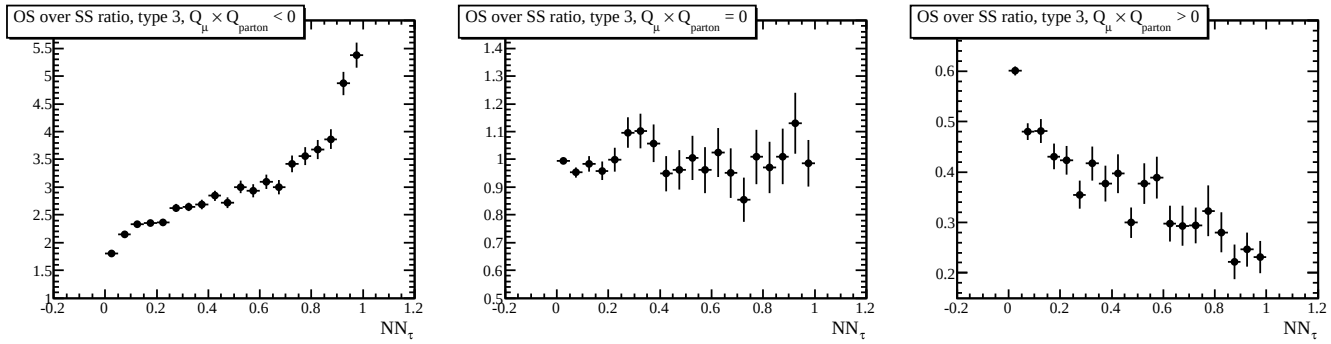

FIG. 2: OS over SS ratio versus NN_τ for the W+jets simulated events (τ type 3). The three categories of events given by the $Q_{\rm parton} \times Q_\mu$ value have a specific behaviour of OS over SS ratio with NN_τ.

First plot of Fig. 3 shows that the OS over SS ratio is different from 1 and is poorly modelled by the plain simulation. To account for Data/MC differences, we use the above physical origins of the behaviour of OS over SS ratio with NN_τ in W+jets events to build a model based on 3 parameters. Then a fit procedure is developped in order to measure simultaneously the charge correlation and the $\tau_{\rm had}$ fake rate, which are related to the model parameters. We first fit the simulation with our model and found a good agreement. Then we apply the procedure to data, and the extracted parameters are used to correct the simulation. The parameters fit is performed in a region free of signal by requiring $\mathrm{NN}_\tau < 0.9$. Fig. 3 shows the OS over SS ratio for the data, the uncorrected simulation and the corrected simulation as well as the correction effect on the $M_T(W)$ distribution in a signal free region.

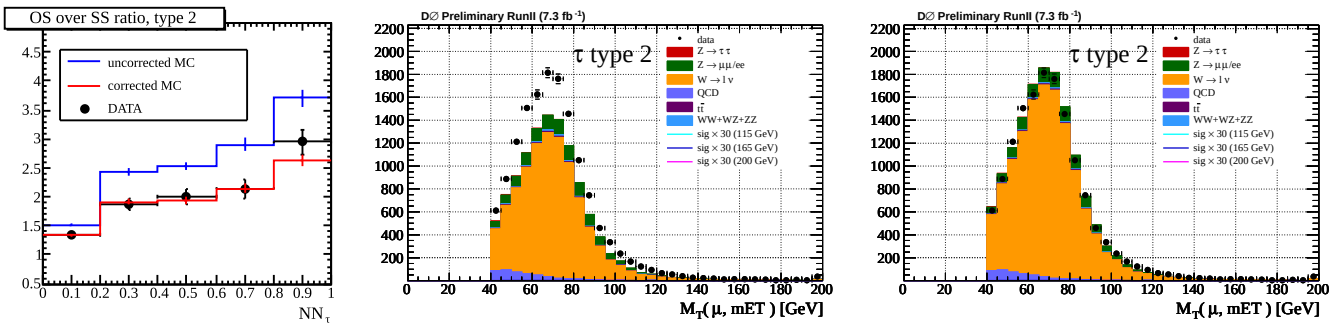

FIG. 3: Left: OS over SS ratio versus NN_τ for data (black dots), uncorrected simulation (blue line) and corrected simulation (red line) for a W+jets enriched sample. Data versus MC comparison of $M_T(W)$ distribution in the SS W+jets enriched sample before correction (middle) and after correction (right). Distributions are plotted for τ type 2.

C. Final selections

At the final selection stage, in addition to preselection criteria, we remove events having $M_T^{\rm min}(l, \not\!\!E_{\rm T}) < 25$ GeV (where $l = (\mu, \tau)$). This cut suppresses a large fraction of Z+jets and MJ background while it has a signal efficiency of 80%, as shown in Fig. 4. This final sample is dominated by W+jets background. Tab. II gives the expected and observed number of events in the final sample. Fig. 5 shows $p_T(\tau)$ and $M_{\rm vis}$ distributions for the final selection.

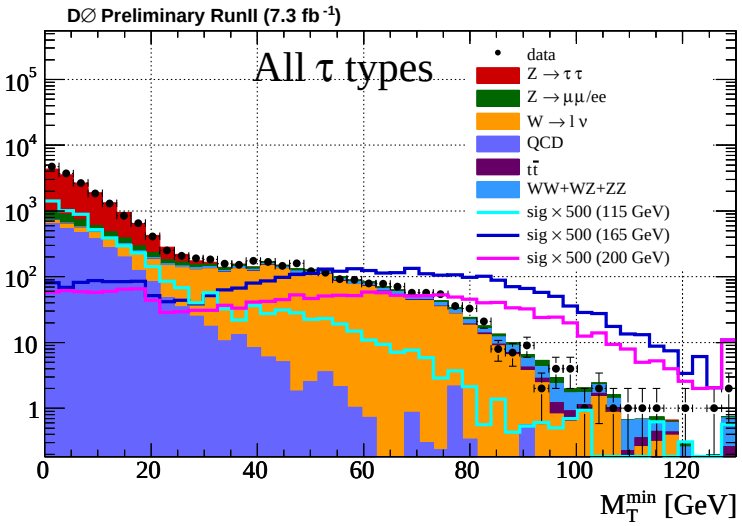

FIG. 4: $M_T^{\rm min}$ distribution at the preselection level for all $\tau_{\rm had}$ types. In order to increase the sensitivity, we keep only events with $M_T^{\rm min} > 25$ GeV.

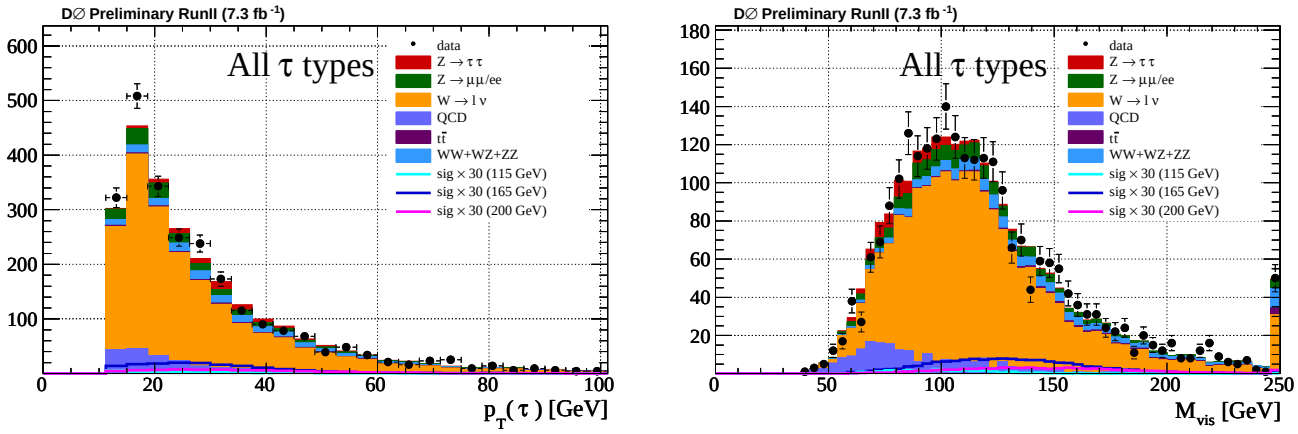

FIG. 5: Data versus MC comparison of $p_T(\tau)$ and $M_{\rm vis}$ distribution in the final sample for all $\tau_{\rm had}$ types.

	$\tau_{\rm had}$ type 1	$\tau_{\rm had}$ type 2	$\tau_{\rm had}$ type 3	all types
$Z(\rightarrow \tau\tau)$	10.1 ± 1.1	54.8 ± 2.7	18.9 ± 1.6	83.7 ± 3.4
$Z(\rightarrow \mu\mu/ee)$	21.0 ± 1.3	91.8 ± 2.7	55.9 ± 2.0	168 ± 3.6
$W(\rightarrow \mu\nu)$	241 ± 9.8	863 ± 15.4	668 ± 11.0	1773 ± 21.3
$t\bar{t}$	4.3 ± 0.2	20.5 ± 0.3	4.1 ± 0.2	28.9 ± 0.4
diboson	28.7 ± 0.8	106 ± 1.5	25.5 ± 0.7	160 ± 1.9
MJ	28.7 ± 3.6	111 ± 7.7	72.0 ± 6.1	212 ± 10.5
Exp. background	334 ± 10.6	1249 ± 17.7	844 ± 12.8	2428 ± 24.3
Data	340	1294	839	2473
Higgs 165 GeV	0.8 ± 0.0	3.8 ± 0.1	0.6 ± 0.0	5.3 ± 0.1

TABLE II: Expected and observed number of events at the final selection.

IV. RESULT

At the final selection level, the sample is dominated by W background. We use a multivariate technique in order to discriminate signal from background. A set a discriminating variables based on specific properties of the signal and/or background are combined in a final Neural Network ($\mathrm{NN_H}$).

A. Multivariate analysis

The backgrounds considered to train $\mathrm{NN_H}$ are Z+jets, W+jets, $t\bar{t}$ and dibosons and the signal is the sum of all Higgs boson production mechanisms. For each Higgs boson mass, we train a dedicated $\mathrm{NN_H}$. Events with a τ_{had} type 1 and 3 are merged while events with type 2 candidates are considered separately. The input variables used to train $\mathrm{NN_H}$ are listed in Tab. III and Fig. 6 shows data versus MC comparisons of these distributions. Fig. 7 shows the final $\mathrm{NN_H}$ distributions trained for a Higgs boson mass of 165 GeV. We define:

- $\hat{s}_{\mathrm{min}} = \left(\sqrt{E^2(\mu,\tau) - p_z^2(\mu,\tau)} + \not{E}_{\mathrm{T}}\right)^2 - p_T^2(\mu,\tau,\not{E}_{\mathrm{T}})$ [23], where $E(\mu,\tau)$ and $p_z(\mu,\tau)$ are respectively the energy and the momentum z component of the (μ,τ) pair;
- $\cos(\widetilde{\theta})$ is the cosine of the angle between the $z-$axis and the muon in the rest frame of the $\not{E}_{\mathrm{T}} + \mu + \tau$ system,
- $\theta(\tau,\mu) = \arccos\left(\frac{\vec{p}_\tau \cdot \vec{p}_\mu}{|\vec{p}_\tau|\,|\vec{p}_\mu|}\right)$ is the angle between the muon and the τ.

NN Analysis Variables	
Object Variables	
p_T of muon	$p_T(\mu)$
p_T of tau	$p_T(\tau)$
charge times pseudo-rapidity of muon	$Q_\mu \times \eta_\mu$
pseudo-rapidity of τ_{had}	η_τ
NN_τ output	NN_τ
Event Kinematics	
invariant mass of both leptons	$M_{\mathrm{inv}}(\mu,\tau)$
minimal transverse mass of leptons and $\not{E}_{\mathrm{T}}$	M_T^{min}
missing transverse energy	$\not{E}_{\mathrm{T}}$
visible mass	M_{vis}
minimum center of mass energy	$\sqrt{\hat{s}_{\mathrm{min}}}$
Number of jets	n^{jet}
Leading jet p_T	p_T^{jet}
Topological Variables	
azimuthal angle between selected leptons	$\Delta\varphi(\mu,\tau)$
azimuthal angle between muon and $\not{E}_{\mathrm{T}}$	$\Delta\varphi(\not{E}_{\mathrm{T}},\mu)$
azimuthal angle between τ and $\not{E}_{\mathrm{T}}$	$\Delta\varphi(\not{E}_{\mathrm{T}},\tau)$
angle between muon and beam axis	$\cos(\widetilde{\theta})$
angle between τ and muon	$\theta(\tau,\mu)$

TABLE III: Variables considered to discriminate signal from backgrounds.

B. Systematic uncertainties

Systematic uncertainties arise from several sources. Experimental uncertainties are evaluated by comparing data control samples to predictions from the simulation. We split the different sources into two categories: those affecting only the normalisation, and those which affect also the shape of the distributions. We include in the first category the uncertainty on the integrated luminosity (6.1%), on the muon identification efficiency (2.3%), on the trigger efficiency (5%), on the τ_{had} identification efficiency (10/4.0/5.0% for τ_{had} type 1/2/3 respectively), on the theoretical Z production cross section (4%), on the $t\bar{t}$ production cross section (10%), on the dibosons production cross section

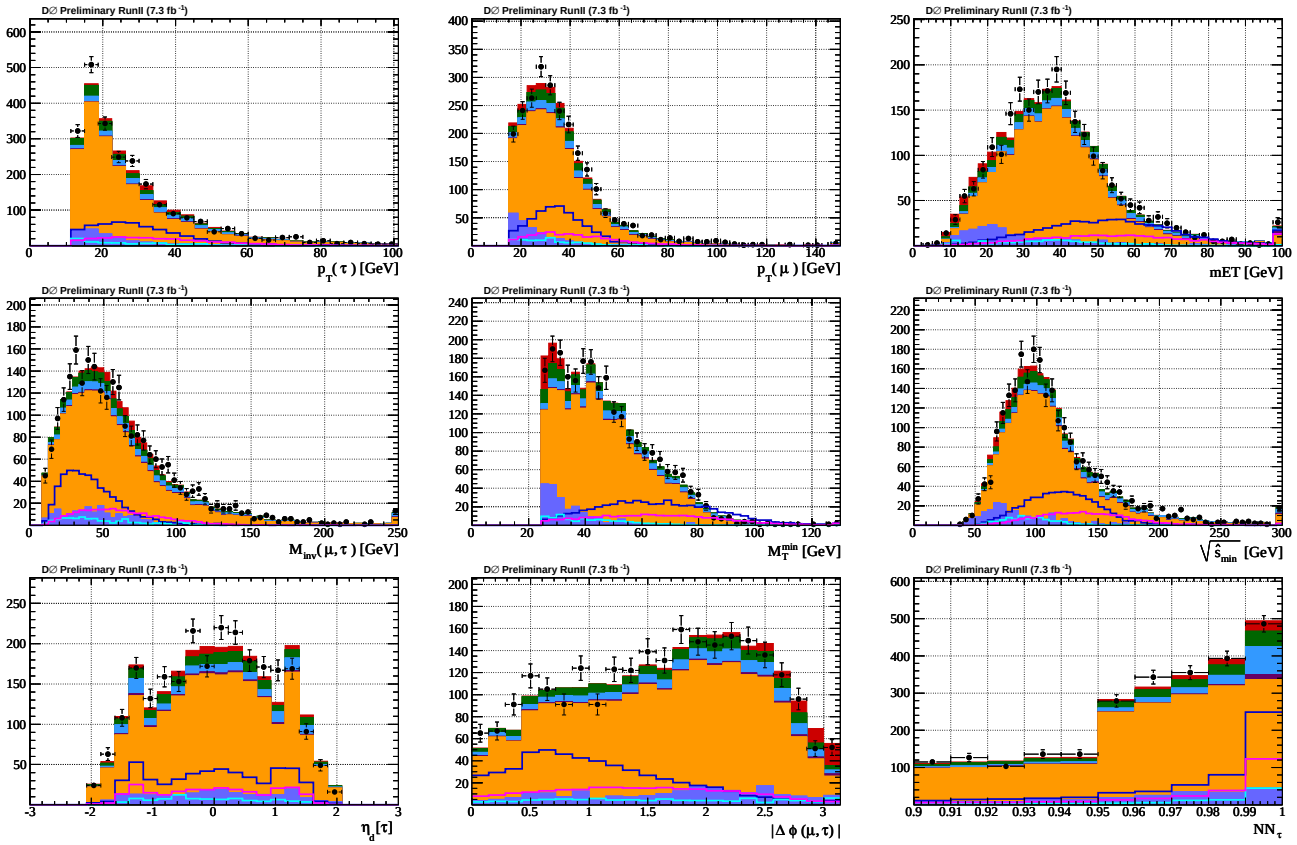

FIG. 6: Data versus MC comparisons of several variables considered to discriminate signal from backgrounds. Distributions are plotted for all τ types and the signal is normalized to 100 × SM. First line: $p_T(\tau)$, $p_T(\mu)$, $\not\!\!E_T$. Second line: $M_{\rm inv}(\mu,\tau)$, $M_T^{\rm min}$, $\sqrt{\hat{s}_{\rm min}}$. Third line: $\eta_{\rm d}(\tau)$, $\Delta\varphi(\mu,\tau)$ and $\rm NN_\tau$.

(7%), on the dibosons p_T modelling (1%), on the gluon-fusion signal modelling (3%) and on W+jets background estimation ($10-15$%). The systematics affecting the shape of $\rm NN_H$ are the uncertainties on the $\tau_{\rm had}$ energy scale (~ 1%), on the jet energy scale ($1-9$ % depending on the process), on the jet energy resolution ($3-9$% depending on the process), on the jet identification efficiency ($1-7$% depending on the process) and on the MJ estimation ($20-50$% depending on the final $\rm NN_H$).

C. Limit on $\sigma(p\overline{p} \to HX) \times \mathcal{BR}(HX \to \mu\tau)$

Final discriminants, as for example shown in Fig. 7, are used as input to a significance calculation using a modified frequentist approach with a Poisson log-likelihood ratio test statistic [24]. In the absence of a significant signal, we derive upper limits at the 95% confidence level on the $\sigma(p\overline{p} \to HX) \times \mathcal{BR}(HX \to \mu\tau)$ as ratio to the SM prediction as a function m_H as shown in Fig. 8.

V. CONCLUSIONS

We performed a search for the SM Higgs boson decaying in the $\mu + \tau$ final state at low jet multiplicity at DØ . This analysis is orthogonal to the other DØ Higgs searches and therefore brings additional sensitivity especially for high mass Higgs searches ($m_H \gtrsim 135$ GeV). We found the data to be compatible with the predicted SM background and placed upper limits on the $\sigma(p\overline{p} \to HX) \times \mathcal{BR}(HX \to \mu\tau)$ as ratios to the SM cross section between 6.6 and 24 for Higgs masses between 135 and 200 GeV.

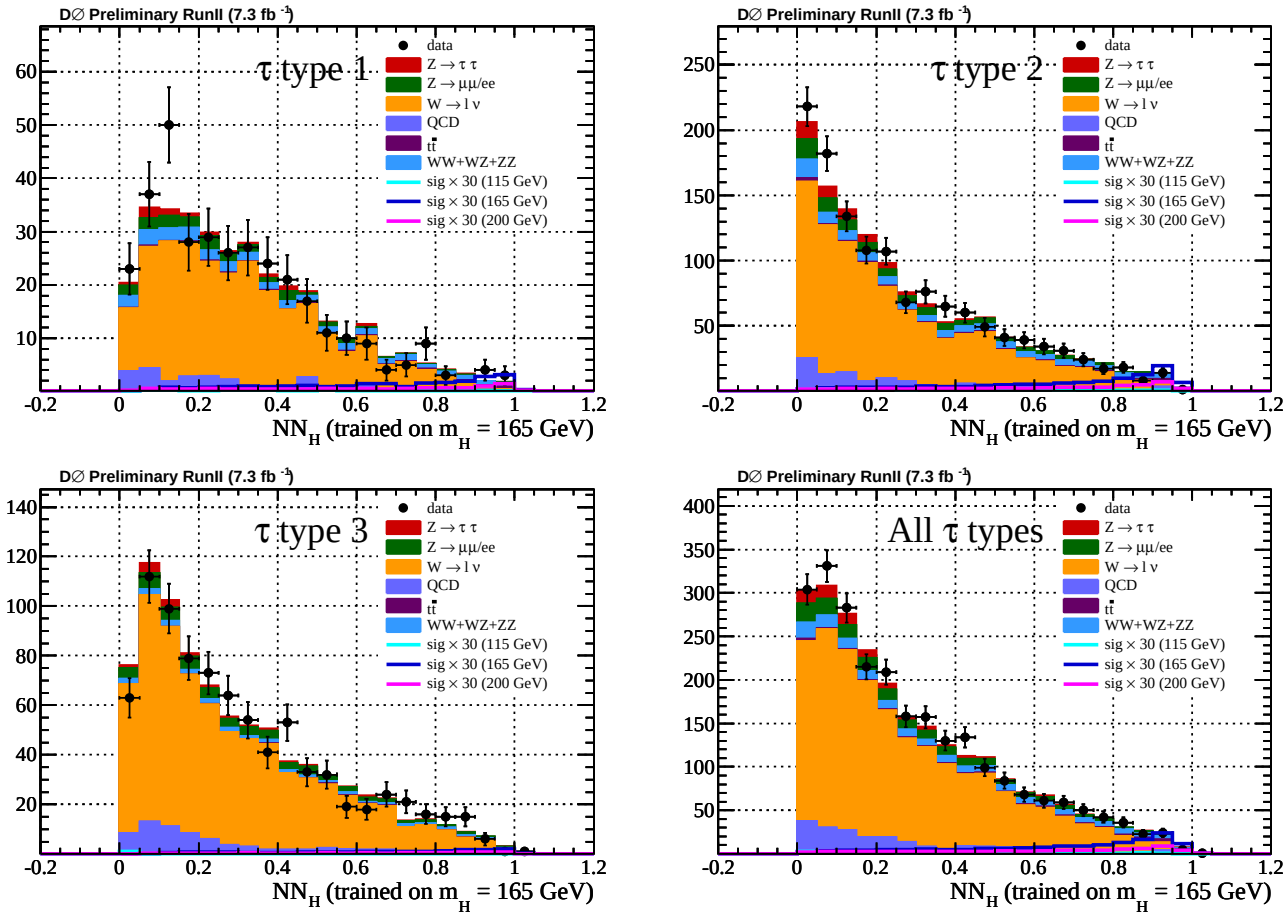

FIG. 7: $\mathrm{NN_H}$ distributions in the final selection for all τ_{had} types.

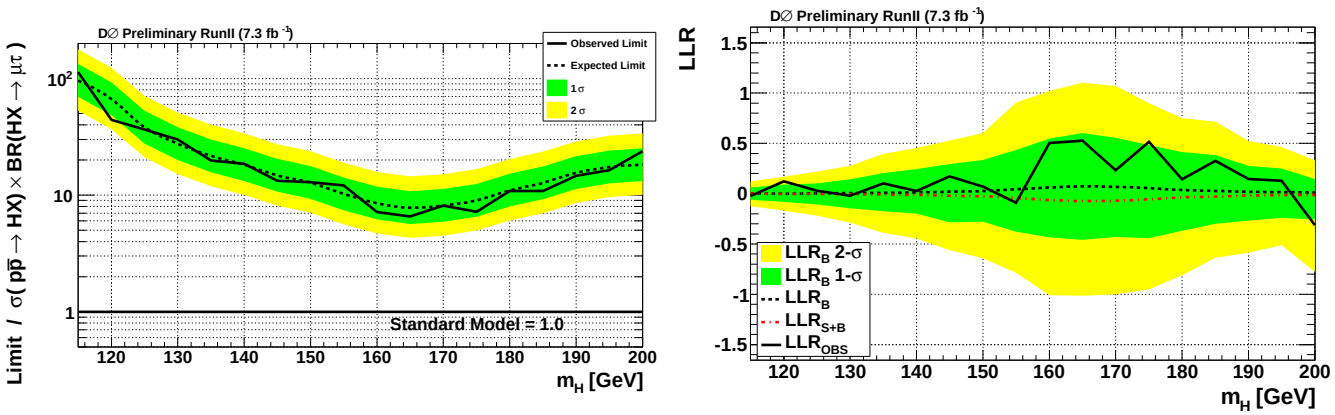

FIG. 8: Left: ratio of the observed and expected exclusion limit at 95% C.L. to $[\sigma(p\overline{p} \to HX) \times \mathcal{BR}(HX \to \mu\tau)]_{\mathrm{SM}}$ as function of m_H. Right: log-likelihood ratio for the background only hypothesis, for the signal + background hypothesis and for the data. Green and yellow bands are the $1\,\sigma$ and $2\,\sigma$ bands respectively.

m_H (GeV)	expected	observed
115	96	110
120	67	44
125	38	36
130	28	30
135	22	20
140	18	19
145	15	13
150	13	13
155	10	12
160	8.5	7.2
165	7.8	6.6
170	8.1	8.1
175	9.0	7.2
180	11	11
185	13	11
190	16	15
195	17	16
200	18	24

TABLE IV: Ratio of the observed and expected exclusion limit at 95% C.L. to $[\sigma(p\overline{p} \to HX) \times \mathcal{BR}(HX \to \mu\tau)]_{\rm SM}$.

Acknowledgments

We thank the staffs at Fermilab and collaborating institutions, and acknowledge support from the DOE and NSF (USA); CEA and CNRS/IN2P3 (France); FASI, Rosatom and RFBR (Russia); CAPES, CNPq, FAPERJ, FAPESP and FUNDUNESP (Brazil); DAE and DST (India); Colciencias (Colombia); CONACyT (Mexico); KRF and KOSEF (Korea); CONICET and UBACyT (Argentina); FOM (The Netherlands); PPARC (United Kingdom); MSMT (Czech Republic); CRC Program, CFI, NSERC and WestGrid Project (Canada); BMBF and DFG (Germany); SFI (Ireland); Research Corporation, Alexander von Humboldt Foundation, and the Marie Curie Program.

[1] The LEP Electroweak Working Group, Status of July 2010, *http://lepewwg.web.cern.ch/LEPEWWG/*.
[2] R. Barate *et al.* [LEP Working Group for Higgs boson searches], Phys. Lett. B **565**, 61, [arXiv:hep-ex/0306033] (2003).
[3] The TEVNPH Working Group (for the D0 and CDF Collaboration), Conference Note 6096-CONF (2010)
[4] V.M. Abazov *et al.* (D0 Collaboration), Conference Note 5332-CONF (2007)
[5] D. De Florian, M. Grazzini, Phys. Lett. **B674** (2009).
[6] C. Anastasiou, R. Boughezal, F. Petriello, JHEP **904** (2009).
[7] V.M. Abazov *et al.* (D0 Collaboration) Phys. Rev. Lett. **96**, 011801 (2006).
[8] T. Andeen *et al.*, FERMILAB-TM-2365 (2007).
[9] V.M. Abazov *et al.* (D0 Collaboration), Nucl. Instrum. Methods Phys. Res. A **565**, 463 (2006).
[10] T. Sjöstrand *et al.*, J. High Energy Phys. **05**, 026 (2006).
[11] P. Bolzoni, F. Maltoni, S.-O. Moch, M. Zaro, Phys. Rev. Lett. **105**, 011801 (2010).
[12] J. Baglio and A. Djouadi, J. High Energy Phys. **1010** 064 (2010).
[13] A. Djouadi, J. Kalinowski and M. Spira, Comput. Phys. Commun. **108**, 56 [arXiv:hep-ph/9704448] (1998).
[14] M.L. Mangano *et al.*, J. High Energy Phys. **307**, 001 (2003).
[15] J. Pumplin *et al.*, J. High Energy Phys. **207** 012 (2002).
[16] D. Stump *et al.*, J. High Energy Phys. **310** 046 (2003).
[17] Z. Was, Nucl. Phys. B - Proc. Suppl. **98**, 96 (2001). Version 2.5.04.
[18] R. Brun and F. Carminati, CERN program library long writeup W5013 1993 (unpublished).
[19] V. M. Abazov *et al.* (D0 Collaboration), Phys. Lett. B **670**, 292 (2009).
[20] G. Blazey *et al.*, arXiv:hep-ex/0005012 (2000).
[21] V.M. Abazov *et al.* (D0 Collaboration), Fermilab-Pub-08/034-E (2008).
[22] V.M. Abazov *et al.* (D0 Collaboration), Conference Note 5845-CONF (2009).
[23] P. Konar, K. Kong, K. T. Matchev, and M. Park, JHEP **0903** (2009).
[24] W. Fisher, FERMILAB report No. FERMILAB-TM-2386-E, 2007.